Intraseasonal Tropical Atmospheric Variability Associated with the Two Flavors of El Nino

D. Gushchina, B. Dewitte

Intraseasonal Tropical Atmospheric Variability Associated with the Two Flavors of El Niño

DARIA GUSHCHINA

Faculty of Geography, Moscow State University, Moscow, Russia

BORIS DEWITTE

Laboratoire d'Etude en Geophysique et Océanographie Spatiale, Toulouse, France

(Manuscript received 5 October 2011, in final form 21 March 2012)

ABSTRACT

The characteristics of intraseasonal tropical variability (ITV) associated with the two flavors of El Niño [i.e., the canonical or eastern Pacific (EP) El Niño and the Modoki or central Pacific (CP) El Niño] are documented using composite and regression analysis. Double space–time Fourier analysis is applied to the NCEP–NCAR zonal wind at 850 hPa (U850) to separate the different components of the ITV in the tropical troposphere, which is then used to define indices of wave activity, and document the spatial pattern of the waves.

It is shown that the ITV characteristics are altered during CP El Niño compared to the typical seasonal dependence of the ITV–ENSO relationship. In particular, while EP El Niño is characterized by enhanced MJO and equatorial Rossby (ER) wave activity during spring–summer prior to the ENSO peak, during CP El Niño, the ITV activity is increased during the mature and decaying phases. It is suggested that ITV is more propitious to the triggering of the EP event; while during the CP event, it contributes mostly to the persistence of positive SST anomalies. The oceanic response of these ITV anomalous patterns is further investigated in the Simple Ocean Data Assimilation (SODA) reanalysis by documenting the seasonal evolution of the intraseasonal equatorial oceanic Kelvin wave (IEKW) activity during the two flavors of El Niño. It is shown that anomalous westerlies associated with ITV may generate the corresponding response in the ocean in the form of anomalous IEKW activity.

1. Introduction

The intraseasonal tropical variability (ITV) is a major component of the atmospheric circulation in the tropics. One usually distinguishes two modes: the so-called coherent Madden–Julian oscillations (MJO) with periods in the 30–90 day band and zonal wavenumbers of 1–3 (Madden and Julian 1972; Zhang 2005) and the equatorial convectively coupled waves [Wheeler and Kiladis 1999 (WK99)] that may be considered as having a ''stochastic'' character relative to the slow oceanic processes. MJO is the dominant tropical intraseasonal mode and a key source of untapped predictability in both the tropics and extratropics (e.g., WK99; Waliser et al. 2003; Waliser 2005; Wheeler and Weickmann 2001). MJO significantly affects a wide range of tropical weather such as the onset and breaks of the Indian and Australian summer monsoons (Wheeler and McBride 2005; Yasunari 1979) and the formation of tropical cyclones (Liebmann et al. 1994; Maloney and Hartmann 2001). It is also tightly linked to the El Niño–Southern Oscillation (ENSO) through its relationship to episodes of westerlies that can trigger downwelling intraseasonal Kelvin waves, a precursor to El Niño onset. Although MJO has been shown to be instrumental in the development of some El Niño events (e.g., Weickmann 1991; Kessler et al. 1995; McPhaden 1999; Zhang and Gottschalck 2002; Lau 2005), its relationship to ENSO is still unclear. For instance, indices of MJO activity were found to be uncorrelated with ENSO indexes (Slingo et al. 1999; Hendon et al. 1999). However, Hendon et al. (2007) clearly demonstrated that enhanced MJO in spring leads by several months the growth of SST in the eastern Pacific (EP), which emerges from the marked seasonal cycle of the MJO activity and phase locking of ENSO

Corresponding author address: Daria Gushchina, Faculty of Geography, Moscow State University, 1 Leninskie Gory, Moscow 119991, Russia.
E-mail: dasha155@mail.ru

DOI: 10.1175/MWR-D-11-00267.1

onset to the seasonal cycle. Despite this strong seasonal dependence, the MJO–ENSO relationship remains ambiguous. Bergman et al. (2001) noted that although MJO was very active preceding the major 1997/98 El Niño, it seemed abnormally inactive prior to the major 1982/83 event. They argue that MJO is responsible for the timing and initial growth of El Niño but not for the generation of the event itself. On the other hand, Roundy and Kiladis (2006) showed that during the 1982 El Niño, an MJO event during May–June excited a Kelvin wave that later was associated with a 20-cm increase in sea level height in less than 2 weeks as it passed Christmas Island in July, and this new state of anomalously high sea level height continued for 7 months. Roundy and Kiladis (2006) also showed that during some specific events, the MJO helped the rapid onset of El Niño conditions while other MJO events were not associated with such dramatic changes in the equatorial oceanic circulation. They hypothesized that the background state of the ocean, which governs the mean wind fields, determines the efficiency of MJO forcing. Seiki et al. (2009) further showed that the atmospheric forcing associated with MJO under westerly and easterly backgrounds has opposite but asymmetric impacts on the ocean, with only westerly forcing being enhanced by the background. They conclude that although MJO is involved in ENSO development, its efficiency remains largely dependent on the ocean and atmosphere background circulation.

In the mean time, the MJO forcing is apparently modulated by ENSO itself (Zhang and Gottschalck 2002; Eisenman et al. 2005; Roundy and Kiladis 2006; Seiki and Takayabu 2007a,b; Kug et al. 2008). Some characteristics of the MJO were shown to change with ENSO: in particular, the zonal pattern of surface westerlies associated with the MJO expands more to the east during the ENSO development phase (Hendon et al. 1998). Roundy and Kiladis (2006) suggested that the effective fetch of the MJO-induced wind stress patch increases during El Niño development with air–sea interaction enhancing and extending the MJO-induced forcing of Kelvin waves as El Niño develops. Later on, Roundy and Kravitz (2009) indicated that weather patterns, including those associated with MJO, tend to evolve differently in association with oceanic Kelvin waves during different phases of ENSO.

Despite the different interpretation of the MJO–ENSO relationship, it has been recognized that MJO events are generated away from the centers of action of ENSO and occur during all phases of ENSO. Reconciling previous results, Roundy and Kravitz (2009) conclude that intraseasonal patterns (MJO type) do not develop at times predetermined by ENSO but rather ENSO affects how they evolve in time and space when they happen to occur. This suggests that ITV might be sensitive to other El Niño properties than just its seasonality, which includes its amplitude, modulation, evolution, and persistence.

The most striking evidence of the change in El Niño characteristics is reflected in the existence of two types of El Niños, as first noted by Yu and Kao (2007): the canonical El Niño as designated by Rasmusson and Carpenter (1982; EP El Niño), which is characterized by SST anomalies located in the eastern Pacific (Niño-3 region), and the so-called central Pacific El Niño [CP El Niño (Kao and Yu 2009); also termed the date line El Niño (Larkin and Harrison 2005), El Niño Modoki (Ashok et al. 2007), or warm pool El Niño (Kug et al. 2009)], with anomalous SST shifted toward the date line and cooler water located to the east and west. Whereas the dynamics of the EP El Niño has been well documented (McPhaden et al. 1998), it is only recently that the community has placed its interest in the mechanisms responsible for the triggering, development, and decay of the CP El Niño. Recent studies (Yu et al. 2010; Yu and Kim 2011) suggested an extratropical sea level pressure (SLP)-forcing mechanism to explain the triggering of the CP El Niño, whereas Yu and Kim (2010b) argued that the decay of the CP El Niño is affected by the warm or cold phase of the EP El Niño. Kug et al. (2009) documented from the National Centers for Environmental Prediction (NCEP) Reanalysis some aspects of the evolution of this kind of event, highlighting differences in the transition mechanism, namely the recharge–discharge process of the equatorial heat content. In particular, they showed that the zonal advective feedback (i.e., zonal advection of mean SST by anomalous zonal currents) plays a crucial role in the development of SST anomalies associated with the CP El Niño, while the thermocline feedback is the key process during the EP El Niño. The different mechanisms of the two flavors of El Niño imply that there are differences in the amplitudes, growth rates, and locations of the SST anomaly, features that may feed back onto the ITV characteristics. As a first step toward the investigation of such feedbacks, it appears necessary to document the ITV characteristics during the two flavors of El Niño. This is the focus of the present paper.

MJO mostly influences the ocean circulation through its imprints on the equatorial westerlies at intraseasonal time scales (periods of 30–90 days). Meanwhile, the higher-frequency disturbances (periods of 7–15 days), named westerly wind bursts (WWB) and represented by intermittent strong westerly winds on the equator, are known to force downwelling Kelvin waves propitious for the development of El Niño (Giese and Harrison

1991; Hartten 1996; Seiki and Takayabu 2007a). However, MJOs and WWBs are not exclusive phenomena. WWBs could in fact be decomposed into a nonlinear combination of many features including MJOs, atmospheric Kelvin waves, equatorial Rossby (ER) waves, cold surges, tropical cyclones, recurving mixed Rossby gravity waves and easterly waves, and mesoscale convective systems, which in turn are superimposed on a basic state of the seasonal cycle and ENSO. The westerly winds of the MJO itself can be part of a WWB, but the MJO also modulates the activity of other waves and tropical cycles, which themselves form part of individual WWB events. For instance, Seiki and Takayabu (2007a) suggested that WWBs are generated in association with the transformation of MJO-related convection, such as the intensified Rossby wave response. Seiki et al. (2009) also demonstrated that WWB–MJO relationships occur through nonlinear interaction between synoptic- and intraseasonal-scale disturbances, which in turn depends on the ENSO phase. In particular, during the El Niño development phase, the background atmosphere circulation and the extension of the warm pool result in the intensification of cyclonic disturbances near the equator within the MJO and contribute to the enhancement of the Rossby wave response (Seiki et al. 2009) as well as the equatorial westerlies.

In a recent study, Gushchina and Dewitte (2011) also show evidence of increased convectively coupled equatorial Rossby waves prior to the development of ENSO, suggesting that, like for MJO, they may be involved in ENSO onset. Interestingly, the variability maximum of the equatorial convectively coupled Rossby waves during the El Niño development phase is observed to the east of the MJO maximum, in contrast to the Rossby waves that form part of the Matsuno–Gill response (Gill 1980) to convection near the equator, which are located to the west of the convection center. Therefore, the peak of Rossby wave activity in the central Pacific appears far from the MJO convection region and may contribute to the westerly wind anomalies induced by the MJO. Note that this does not mean that these Rossby waves are fully independent of the MJO. Kiladis and Wheeler (1995) and Matthews and Kiladis (1999) have demonstrated that extratropical waves propagating into the tropics of the eastern North Pacific basin force equatorial Rossby waves, which then move westward and couple to convection. These extratropical waves propagate into the tropics in regions of upper-level westerly winds. These westerly winds in turn depend on the seasonal cycle, ENSO state, and MJO; therefore the MJO can influence where and when the equatorial Rossby waves form.

Gushchina and Dewitte (2011) further show that the causative relation between ENSO and ITV is strongly dependent on the ENSO amplitude itself, consistent with results by Roundy and Kravitz (2009) and Tang and Yu (2008). In particular, the periods of strong ENSO amplitude are characterized by increased activity in both MJO and the equatorial Rossby waves in the western-central Pacific in spring–summer preceding El Niño, while the seasonal phase locking between ENSO and ITV exhibits significantly different characteristics during periods of low ENSO amplitude. In particular, prior to the El Niño peak, the MJO and Rossby wave signal is weaker and shifted to the eastern Pacific while during the subsequent year the MJO activity is maintained during the whole year. Such modulation of the ITV–ENSO relationships may result from various ocean–atmosphere feedbacks implemented in the evolution of the two El Niño flavors. It calls for a detailed investigation of the ITV amplitude, evolution, and propagation characteristics associated with the two types of El Niño, which this paper addresses.

The remainder of the paper is organized as follows: first the data and the methods are presented (section 2). Then section 3 presents the results of the composite analysis. Section 4 contains a discussion followed by concluding remarks.

2. Dataset and method descriptions

a. Datasets

The daily zonal wind at 850 hPa (U850) was obtained from the NCEP–National Center for Atmospheric Research (NCAR) reanalyses (Kalnay et al. 1996; Kistler et al. 2001). The Hadley Centre Global Sea Ice and Sea Surface Temperature dataset (HadISST; Rayner et al. 2003) archives are used to derive monthly Niño-3 (5°S–5°N, 150°–90°W) and Niño-4 (5°S–5°N, 160°E–150°W) SST anomalies as well as estimate the position of the 28°C isotherm at the surface.

An estimation of the oceanic intraseasonal Kelvin waves was derived from the Simple Ocean Data Assimilation (SODA) reanalysis (2.1.6 version) (Carton and Giese 2008) over the period 1958–2008. The method for deriving the Kelvin waves is similar to that of Dewitte et al. (2008) and consists of projecting the simulated variability onto the theoretical vertical mode and meridional Kelvin–Rossby mode functions. The latter are derived from the SODA mean vertical stratification at each grid point along the equator and time step [a slowly varying density field is considered (low-pass filtered at 7 yr); the reader is invited to refer to Dewitte et al. (2008) for more details about the method]. An estimate of the intraseasonal Kelvin wave is provided that somehow takes into account dispersion effects associated with the zonally and temporally

(low frequency) varying stratification. The 5-day mean anomalies are referenced to the running monthly mean, which provides variability time scales in the range between 10 and 120 days. Intraseasonal anomalies are therefore calculated by removing from the total field, the monthly averaged values interpolated on a 5-day temporal grid through spline functions. This method is similar to the one used to compute intraseasonal anomalies of the atmospheric fields and follows Lin et al. (2000).

Note that SODA tends to underestimate the amplitude of the intraseasonal temperature variability along the equator as compared to tropical atmosphere ocean (TAO) observations (Carton and Giese 2008). Despite this bias, features relevant for the understanding of the intraseasonal Kelvin wave activity and its relationship to ITV can be determined, as will be seen in section 3. Hereafter, the oceanic intraseasonal equatorial Kelvin wave will be referred to as IEKW.

b. Methods

To document the ITV patterns we use a technique similar to that in WK99. It is based on the decomposition of the symmetric and antisymmetric components of the zonal wind at 850 hPa (U850) in the frequency–wavenumber space for the period 1958–2010. Inversed Fourier transform is then used to recompose the signal in the desired frequency and wavenumber bands. The frequency and wavenumber intervals were derived from the normalized space–time spectrum for U850 and are centered on the spectral maximum of U850 (cf. Gushchina and Dewitte 2011). These are a period of 30–96 days for MJO-zonal wavenumbers 1 to 3, a period 10–50 days for equatorial Rossby waves–zonal wavenumbers -1 to -8, and a period 3–30 days for Kelvin waves–zonal wavenumbers 1 to 9 [with negative (positive) zonal wavenumber corresponding to the westward- (eastward) propagating waves]. To avoid the effect of nonstationarity of the initial time series, direct and inverse Fourier transform was calculated over a 5-yr running window, retaining the central values of the recomposed signal. The recomposed signal therefore spans the period of 1960–2008. The amplitude of equatorial waves was computed by taking the root-mean-square (rms) of the MJO, Kelvin, and equatorial Rossby-filtered U850, with the rms computed in a running window dependent on the wave's type (90, 48, and 30 days for MJO, equatorial Rossby, and Kelvin waves, respectively). Then the running rms was averaged monthly. The amplitude time series were first equatorially averaged (5°S–5°N) at each point of longitude, and to obtain the indices of ITV activity, the amplitude time series were averaged over the regions where the maximum ITV–ENSO relationship was observed (Gushchina and Dewitte 2011): the western Pacific (5°S–5°N, 120°E–180°) for MJO and Kelvin waves, central Pacific (5°S–5°N, 140°E–160°W) for Rossby waves, and eastern Pacific (5°S–5°N, 160°–100°W) for Kelvin waves.

To separate the characteristics of the ITV during the two flavors of El Niño, the composite analysis is used. The CP and EP years are selected using the method proposed by Yeh et al. (2009), namely based on the values of the Niño-3 and Niño-4 indexes with a threshold of 0.5°C during the November–January (NDJ) season to define that an El Niño is occurring. Over 1960–2008, this leads to the selection of six CP events (1968/69, 1990/91, 1994/95, 2002/03, 2004/05, and 2006/07) and five EP events (1965/66, 1972/73, 1976/77, 1982/83, and 1997/98). Note that the 1986/87 event was not considered in the analysis because this event evolves as an EP event at the developing phase and turns toward the CP type at the mature phase. For comparison purposes, eight La Niña events (1970/71, 1973/74, 1975/76, 1984/85, 1988/89, 1998/99, 1999/2000, and 2007/08) were selected based on the value of the Niño-4 index being less than -0.5°C in NDJ. The significance of the composites was estimated using the bootstrap method (Efron 1982). The method is equivalent to Monte Carlo testing (cf. Björnsson and Venegas 1997) and consists of creating a surrogate dataset—a randomized dataset of (six) CP and (five) EP events—by scrambling 49 years in the time domain. The composite analysis is then performed on the scrambled dataset. The same procedure of scrambling the dataset and performing the analysis is repeated 300 times, each time keeping the value of the CP and EP composites (in the space and time domains). Then the difference between the CP and EP composites is calculated for the 300 samples and the distribution of these differences is obtained. The latter is used for deriving the significance level of the difference between the composites. Because of the relatively limited number of events over the 49-yr-long period, it is difficult to reach a high level of significance, so the 75% level was selected to highlight the space–time domain where the results are discussed. Such criteria are used because we diagnose the significance of the difference between the CP and EP composites rather than the significance of one composite (either CP or EP) with respect to the mean seasonal condition, which is a much more stringent test.

To check the consistency of our results, we also used the indices of CP and EP El Niño as recently defined by Takahashi et al. (2011). They define these so-called E and C indices based on the linear combination of the first two EOF-associated time series of the SST

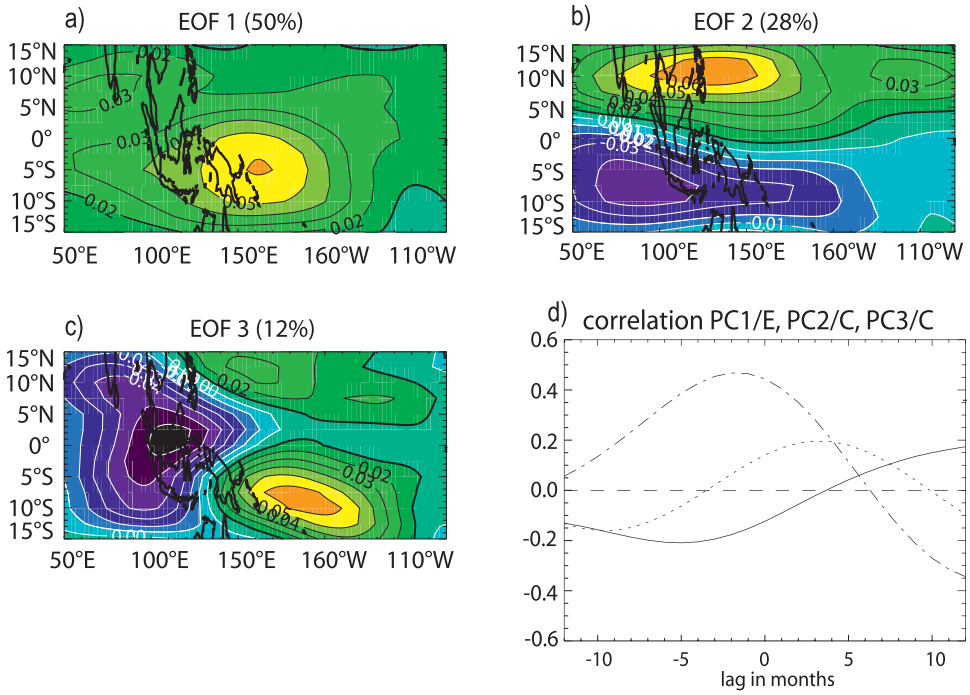

FIG. 1. (a)–(c) First three EOF modes of the MJO-filtered U850 (see text). (d) Correlation between C–E indices and times series associated with the EOF modes (PC1–E: solid line, PC2–C: dotted line, PC3–C: dashed–dotted line). Negative lags: MJO lags, positive lags: MJO leads.

anomalies in the tropical Pacific (PC1 and PC2). Takahashi et al. (2011) noted that the phase space of (PC1, PC2) forms a ''boomerang'' shape that provides favorable directions over which a lot of variance of the SST anomalies can be projected (see their Fig. 2). They thus propose rotating PC1 and PC2 by 45° to interpret the variability within a basis that better fits with the boomerang shape. This operation allows for grasping more variance for the regime associated with the El Niño Modoki event as compared to the El Niño Modoki Index (EMI) proposed by Ashok et al. (2007) (i.e., PC2). In that sense, the E and C indices account better for the nonlinear character of ENSO because they represent distinct regimes of the ENSO variability. Whereas the E index accounts for the extreme El Niño events (EP type), the C index grasps the variability associated with the CP El Niño and La Niña events. These indices, independent by construction (i.e., their correlation is zero), can be conveniently used for regression analyses (see Takahashi et al. 2011 for more details). To differentiate CP El Niño from La Niña events, conditional regression analysis was performed with the C index considering periods when its value is positive and negative, respectively. However, the conditional analysis is applied only for small time lags to avoid mixing information from independent years. A Student's t test is used (Spiegel 1990) to compute the confidence level for the regression. The degree of freedom is $n - 2$, where n is the number of observations.

As a first step and to illustrate our methodology, we verify that the MJO variability is not linked to the ENSO variability in a straightforward manner. The MJO variability (running-windowed rms of MJO filtered U850) is first extracted following the method described above for the whole tropical Pacific (15°S–15°N, 50°E–90°W). The signal exhibits strong seasonal variability at some periods in the off-equatorial region (not shown), indicative of a significant modulation of the seasonal cycle at decadal time scales. This seasonal variability modulation is filtered out using the wavelet decomposition, retaining time series associated with wavelet power for frequencies ranging from 1.5 to 8 yr^{-1}. An EOF analysis is then performed on the filtered MJO signal over the domain of the tropical Pacific (15°S–15°N, 50°E–90°W). The EOF patterns for the first three modes are presented in Fig. 1. The first mode represents the interannual modulation of the MJO activity, whose variability maximum is located in the Southern Hemisphere over the western Pacific. The second mode shows the interannual modulation of cross-equatorial MJO seasonal displacement with an asymmetric enhancement of MJO activity in the Northern and Southern Hemispheres. Note that these first two modes are weakly correlated with El Niño indices (Fig. 1d). The correlation between PC1 (PC2) and

the C (E) index is very low (not significant) while the correlation between PC1 and the E index and PC2 and the C index reaches significant values, although very low (−0.23 at lag −5 months for PC1–E and 0.21 at lag 4 months for PC2–C). It does, however, suggest that 4–5 months after the EP El Niño peak, the MJO activity decreases over the western tropical Pacific, while intensification of MJO in the Northern Hemisphere precedes by 4 months the CP El Niño. Only the third EOF mode time series (PC3) exhibits a significant and relatively large correlation with the C index (see dashed–dotted line in Fig. 1d). The spatial pattern of the third EOF demonstrates the west–east displacement of the MJO activity center over the western Pacific and the Australian region. During CP El Niño, the MJO activity is amplified in the western Pacific and suppressed over the Indian Ocean and Australia and vice versa (peak correlation of 0.50 at lag −1 month).

The relatively low correlation values found between ENSO indices and the statistical dominant modes of the MJO activity over the tropical Pacific are indicative of the strong seasonal dependence between ITV and ENSO (Hendon et al. 2007) and also the likely different characteristics of the MJO pattern during the different flavors of El Niño.

3. Results

As a first step, we analyze the composites of the seasonal evolution of the various components of the ITV for the two flavors of El Niño and for La Niña (Fig. 2). They can be compared to the mean seasonal cycle for the whole period. Peculiarities of the seasonal evolution of the MJO and ER pattern over the tropical Pacific are also discussed. We then discuss the coupling of the convective atmospheric waves with the intraseasonal oceanic Kelvin waves during the different flavors of El Niño.

a. MJO activity

For MJO, the differences between CP and EP as well as the mean seasonal cycle are marked: whereas the MJO activity is intensified in boreal spring prior to the El Niño peak phase during both El Niño flavors (with, however, a lower signal for the CP event), the MJO activity during the mature and decaying phases of the event changes drastically between the two types of El Niño. During EP El Niño, the MJO activity is reduced compared to the mean seasonal cycle during these particular ENSO phases (Fig. 2a). The negative anomalies of MJO following the EP peak are obviously seen in Fig. 3b. Conversely, under CP conditions, the mature and decaying phases are characterized by anomalously large MJO activity (Fig. 2b). Note, however, that just after the CP El Niño peak, the MJO activity drastically decreases, as can be seen from the negative anomalies in February–March of El Niño years (Fig. 3g). However, from May, the MJO is significantly amplified in the equatorial western and central Pacific. The enhanced MJO activity during the decaying phase of the CP event may contribute to the persistence of equatorial westerlies. The running skewness of ITV-filtered data was estimated in a similar manner to that for the running rms. The results indicate that the anomalous peaks in variability are preferentially associated with westerlies because anomalies are positively skewed (not shown). In turn, the anomalous westerlies induce the ocean forcing (see below), which results in a slower damping of SST anomalies under CP conditions (Figs. 3a,f).

In addition, MJO activity is reduced over the entire Pacific during the developing and decaying phases of the La Niña event as illustrated Fig. 2c. The maximum of MJO activity appears in the equatorial western Pacific only during the peak phase of La Niña. It is associated with the enhanced convection over the warm pool, which has its westernmost position under La Niña conditions.

To estimate the evolution of the MJO/ENSO relationship over the entire tropical Pacific, Fig. 4 presents the regression maps of the MJO variance upon the C and E indices. It confirms that the relationship between MJO and ENSO is enhanced during the CP event as compared to the EP event, with, in particular, an eastward and southward migration of the region of significant positive values as a function of lead time during the CP event. Note that the C index also accounts for the La Niña events (Takahashi et al. 2011) so that the regression pattern of Figs. 4h–n accounts for the combined influence of the CP event and La Niña event. For instance, the negative values to the west of the date line, which are well marked at lags of 6–9 months, are likely due to the enhanced convection and associated MJO over this region under La Niña conditions. To exclude the influence of the La Niña event, the conditional regression analysis (i.e., considering only the periods when C is positive) was performed. The results reveal similar patterns to those in Figs. 4j–l (not shown). Interestingly, the MJO–C positive regression pattern over the Southern Hemisphere matches the South Pacific convergence zone (SPCZ) location, suggesting an MJO amplification within the SPCZ during the CP event. This is consistent with the increase in tropical cyclone number within the SPCZ during the fall–winter of El Niño (Sokolikhina et al. 2006), the latter being associated with the positive MJO phase as suggested by Liebmann et al. (1994). Note also the positive regression pattern during the CP event

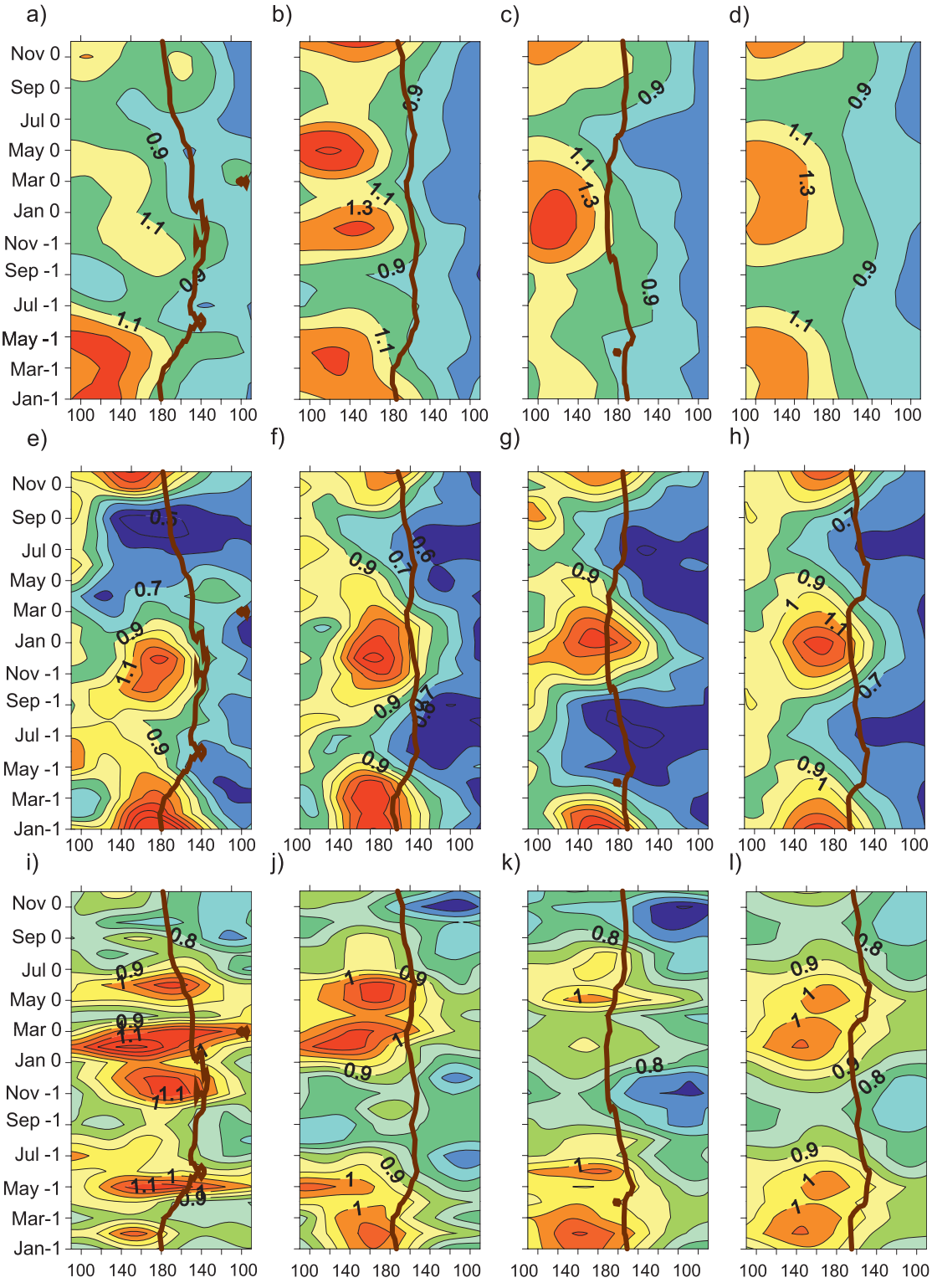

FIG. 2. Time–longitude cross sections of running variance (rms) of (a)–(d) U850 filtered MJO, (e)–(h) equatorial Rossby waves, and (i)–(l) Kelvin waves. Composites for (a),(e),(i) EP El Niño (1965/66, 1972/73, 1976/77, 1982/83, 1997/98), (b),(f),(j) CP El Niño (1968/69, 1990/91, 1994/95, 2002/03, 2004/05, 2006/07), (c),(g),(k) La Niña (1970/71, 1973/74, 1975/76, 1984/85, 1988/89, 1998/99, 1999/2000, 2007/08), and (d),(h),(l) mean seasonal cycle (averaged over 1960–2008). January 0 corresponds to the peak of the events. Contour interval is 0.1 m s^{-1} for Kelvin waves and 0.2 m s^{-1} for MJO and Rossby waves. The brown thick line indicates the mean position of the 28°C isotherm for the composite years.

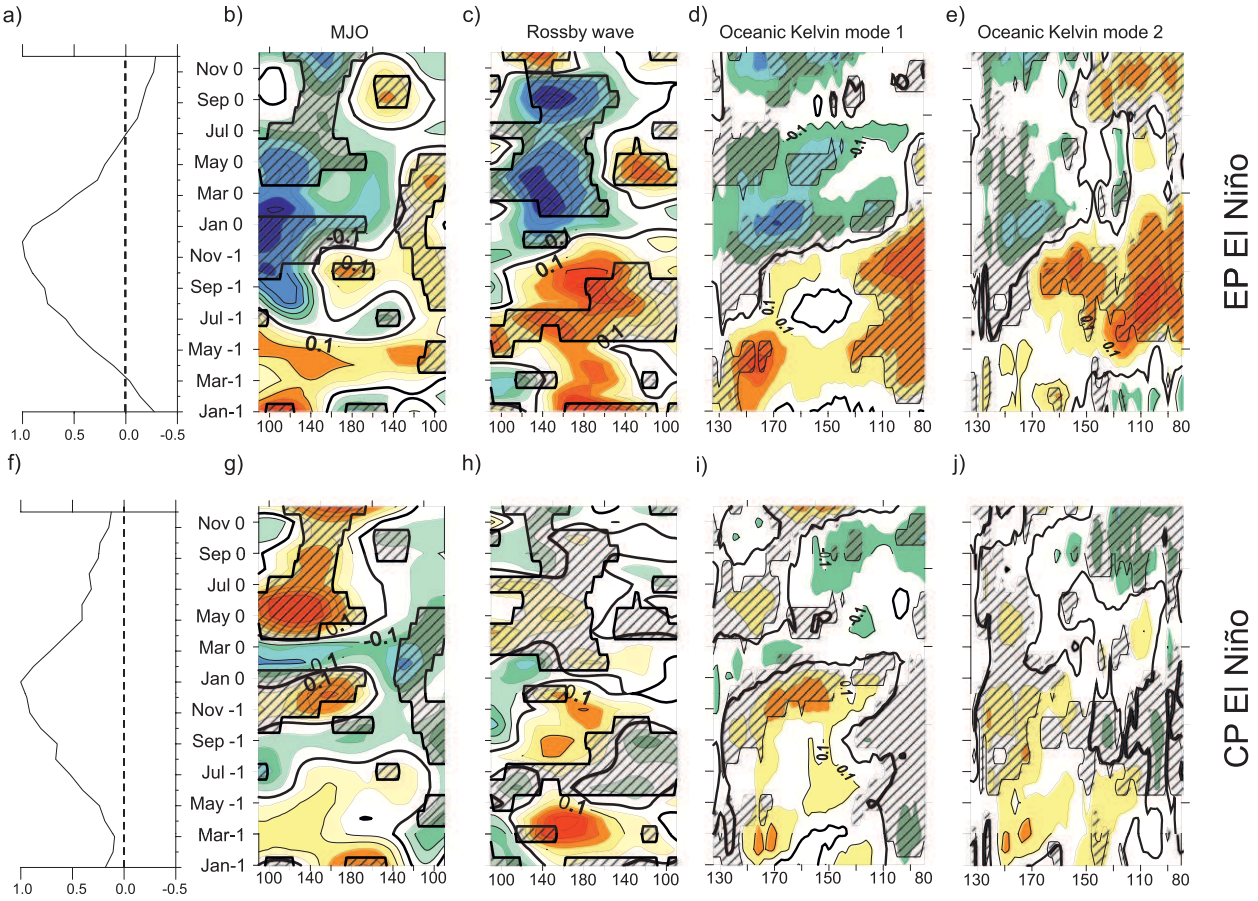

FIG. 3. Composite SST anomalies averaged over (a) the Niño-3 region (5°S–5°N, 150°–90°W) for EP El Niños and (f) the Niño-4 region (5°S–5°N, 160°E–150°W) for CP El Niño normalized by the maximum value of the composite anomalies (2.21° and 0.87°C, respectively). Time–longitude cross sections of anomalies of running variance (rms) for (b),(g) MJO filtered, (c),(h) equatorial Rossby waves filtered U850, (d),(i) first baroclinic-mode oceanic Kelvin wave, and (e),(j) second baroclinic-mode oceanic Kelvin wave. Composites for (a)–(e) EP El Niño (1965/66, 1972/73, 1976/77, 1982/83, 1997/98) and (f)–(j) CP El Niño (1968/69, 1990/91, 1994/95, 2002/03, 2004/05, 2006/07). Contour interval is 0.05 m s^{-1} for MJO and Rossby waves, 0.1 cm for the first mode of the Kelvin wave, and 0.05 cm for the second mode of the Kelvin wave. The regions in the *x–t* space for which the difference between EP and CP composites is significant at the 75% level are shaded.

that expands toward the Northern Hemisphere around 150°W with no counterpart during the EP event. The Northern Hemisphere maximum perfectly coincides with the CP-associated anomalous precipitation pattern evidenced by Ashok et al. [cf. Fig. 9 of Ashok et al. (2007)].

During the EP event, from the peak phase (Figs. 4d–g), the MJO activity over the entire tropical western and central Pacific is reduced, resulting in a negative value for the regression between the E index and MJO activity.

b. Convectively coupled atmospheric Rossby wave activity (ER)

Whereas most attention has been drawn to the relationship between ENSO and MJO, the Rossby wave has also been suggested to be instrumental in the development of equatorial westerlies. Seiki et al. (2009) demonstrated that during pre–El Niño conditions, the Rossby wave response is dominant in the mean wind structure of the MJO, while Seiki and Takayabu (2007a) suggested that westerly wind bursts are generated in association with the transformation of MJO convection, such as the intensified Rossby wave response, over the background westerly region near the equator. Gushchina and Dewitte (2011) evidenced the strong correlation between the intensity of convectively coupled equatorial Rossby waves and westerly wind anomalies along the equator in summer–fall preceding an ENSO peak. Although energetic in a higher-frequency range than the MJO (WK99), ER variance has a marked seasonal evolution (Fig. 2h) comparable to that of the MJO. Its deviation from the mean seasonal cycle during

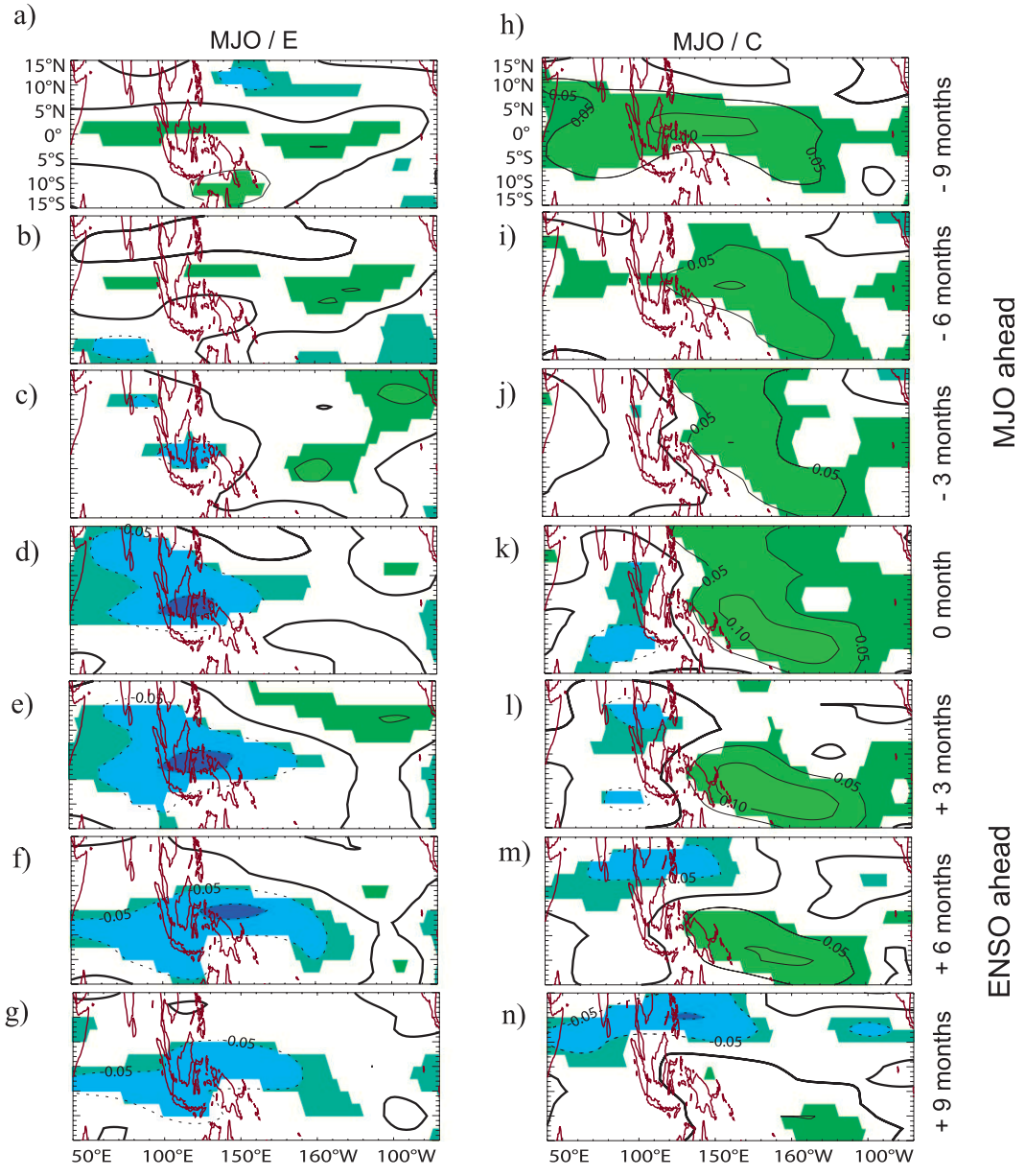

FIG. 4. Lag regression of the MJO-filtered U850 running variance (rms) upon the (a)–(g) E and (h)–(n) C indices normalized by respective rms. The regression significant at the 90% level is colored. Contour interval is every 0.05 unit and units are 0.92 (0.82) m s^{-1} for the lhs (rhs). The thick black line, which is not labeled, indicates the zero line.

the different ENSO phases (Figs. 2e,f) is, however, less pronounced than for MJO. Still, significant differences of the anomalous ER activity can be observed between the two flavors of El Niño. During the CP event, the strongest anomalies occur in spring (Fig. 3h), while EP events are characterized by maximum anomalies in summer–fall (Figs. 3c). The latter is due to the earlier intensification of the Rossby waves as compared to the mean seasonal cycle (Figs. 2e,h). After the peak phase of ENSO, the anomalous ER activity becomes negative for the EP event, whereas it remains slightly positive for the CP event, suggesting that ER may contribute to the persistence of equatorial westerlies (the ER anomalies like the MJO are positively skewed) and the associated oceanic response. Noteworthy, the ER has a center of action more to the east compared to MJO, but its contribution to the oceanic Kelvin response may be specific in terms of its contribution to the baroclinic modes (i.e., mode 2 may be favored in association with ER-related forcing) (see next section). The La Niña condition corresponds to

a slight intensification of the seasonal maxima of ER activity: the maxima appear at the same time but their amplitude is somewhat larger than for the mean seasonal cycle, especially in January–February (1.4 vs 1.3 m s^{-1}) (Figs. 2g,h).

c. CAKW activity

The direct atmospheric response to the oceanic heat forcing consists of the convective atmospheric Kelvin waves (CAKWs) and Rossby waves observed to the east and west of the heat source, respectively (Gill 1980). Atmospheric convectively coupled Kelvin waves have a wide spectrum of variability from daily to monthly time scales (see WK99). However, at these frequencies the oceanic Kelvin wave dissipates (and propagates vertically) very rapidly (Philander 1978), therefore it is not likely that direct coupling between convective Kelvin waves and oceanic Kelvin waves takes place. The stronger expression of these atmospheric Kelvin waves over the Pacific basin during El Niño is more likely associated with increased amplitude in convection caused by the warmer SST background state. The different SST backgrounds associated with the two El Niño flavors may therefore result in different atmospheric Kelvin wave patterns. This is seen in Figs. 2i,j, which show the seasonal evolution of the CAKW activity during the two types of El Niño. During the EP event, the Kelvin wave signal propagates toward South America while it does not penetrate to the east of 160°W during the CP event (Figs. 2i,j). The CP composite corresponds to a clear intensification of the seasonal cycle both prior to and after the El Niño peak phase. During La Niña, the CAKW activity evolution does not differ significantly from the mean seasonal cycle but the amplitude of the CAKW peaks is lower than in the seasonal cycle (Fig. 2k).

d. Relationship with the oceanic intraseasonal Kelvin wave

As a consistency check with the previous analysis, it is now interesting to investigate the seasonal evolution of the IEKW activity during the two flavors of El Niño, considering that MJO and ER have a spectrum of variability propitious for the forcing of oceanic Kelvin waves. Following the same methodology as that for calculating ITV activity, the running variance of the IEKW is estimated over 3-month-length windows. Figures 3d,e,i,j display the deviation from the mean seasonal cycle of the climatological running variance of the IEKW during the EP and CP years and for the first two baroclinic modes. It can be directly compared to the anomalous MJO and ER activity (Figs. 3b,c,g,h) to show how the convective activity projects onto the ocean circulation during the two different types of El Niño.

Figure 3 demonstrates that positive MJO anomalies prior to the ENSO peak clearly induce the positive anomalies of the first baroclinic-mode oceanic Kelvin wave during both types of events. In particular, the intensification of MJO activity in March–May (year −1) in the western Pacific has a clear counterpart in the IEKW activity of the first baroclinic mode for the EP event, while for the CP event, the intensification of the first baroclinic-mode IEKW activity takes place at the peak phase, like for the MJO activity. The second baroclinic-mode IEKW activity may result from the modal dispersion from the first to the second baroclinic mode (Dewitte et al. 1999) since the positive anomalies of the IEKW for the second baroclinic mode are found mostly in the eastern Pacific and do not exhibit a clear counterpart in the MJO activity anomaly. It may also result from direct wind stress forcing associated with the ER since the location of the positive ER anomalies fits better with the location of the positive anomalies of the second baroclinic-mode IEKW activity, especially for the EP event. Overall, for the EP event, the MJO contribution is better projected onto the first mode of the oceanic Kelvin wave (Figs. 3b,d) while ER projects on the second mode (Figs. 3c,e). During the CP event, the positive anomalies of both ITV components are mostly associated with the growth of the first mode of IEKW, while the imprint on the second mode is unclear.

During the decaying phase of the EP event, the suppressed ITV activity results in negative anomalies of the IEKW variance (Figs. 3d,e). On the other hand, the CP event is characterized by enhanced ITV during its decaying phase in the western Pacific, which contributes to the slight increase in IEKW activity (Figs. 3i,j) around April–July (year 0). This may explain the slower damping of SST during the CP event than during the EP event (Figs. 3a,f).

4. Discussion and conclusions

The ITV characteristics during the two flavors of El Niño are documented. Double space–time Fourier analysis is applied to identify the ITV components following the method of WK99. The composites of the seasonal evolution of MJO and convectively coupled equatorial Rossby and Kelvin waves are presented for the eastern Pacific and central Pacific El Niño as well as for La Niña. It is argued that the seasonal dependence of the ITV–ENSO relationship (Hendon et al. 2007) is altered for the CP El Niño compared to the EP El Niño. In particular, the enhanced ITV activity is mostly prominent during the development phase of the EP El Niño,

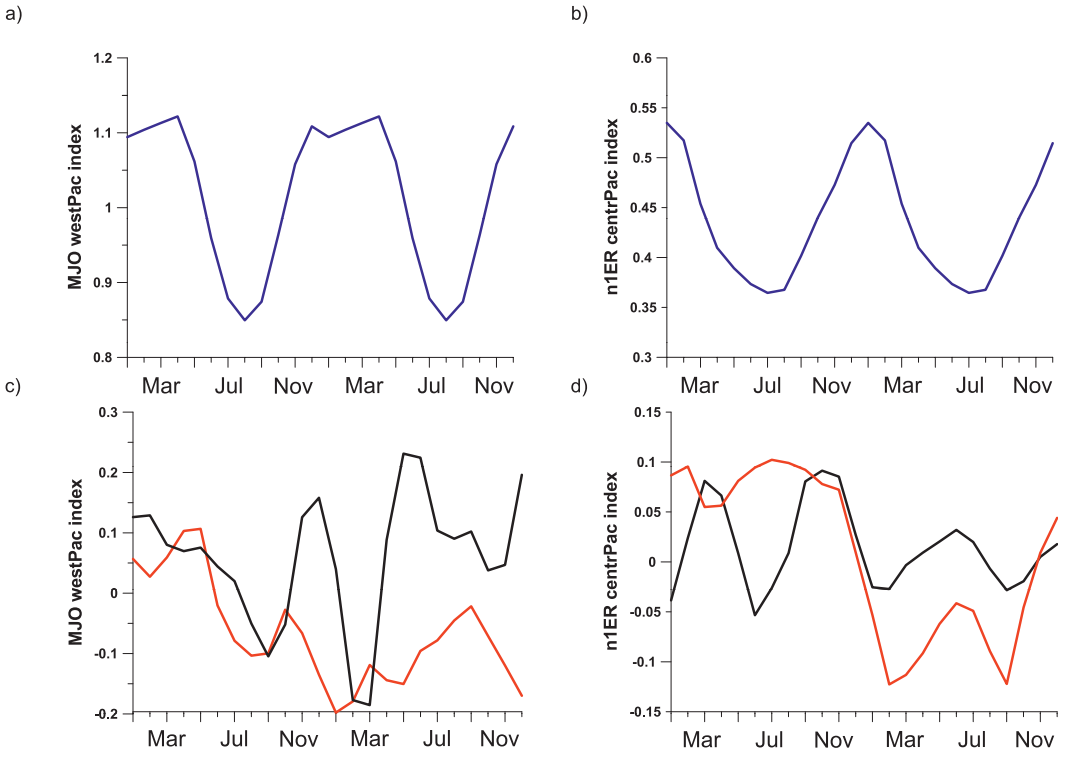

FIG. 5. Running variance (rms) of U850-filtered (a),(c) MJO averaged over the west Pacific region (5°S–5°N, 120°E–180°) and (b),(d) equatorial Rossby waves averaged over central Pacific region (5°S–5°N, 140°E–160°W). (a),(b) Mean seasonal cycle and (c),(d) deviation from the mean seasonal cycle during the EP event (1965/66, 1972/73, 1976/77, 1982/83, 1997/98; red line) and CP event (1968/69, 1990/91, 1994/95, 2002/03, 2004/05, 2006/07; black line).

while during the CP El Niño it takes place at the peak phase of the event and during its decaying phase, potentially contributing to the slower damping of SST anomalies. After the peak of the EP event, the ITV activity is reduced (lower than its climatological value) in the central Pacific. Our results suggest that the MJO activity, but also the ER activity, are influential for the maintenance (persistence) of the warm SST anomaly in the central Pacific during the CP event, while they mostly contribute to the growth of SST during the development of the EP El Niño. For a summary, we provide Fig. 5, which displays the composites of the deviation of the MJO and ER activity indices in the western-central equatorial Pacific from their mean climatological value. The largest difference between the CP and EP events is observed during the peak and decaying phases of the El Niño, with the MJO and ER activity composite exhibiting a positive anomaly and no deviation from the seasonal cycle, respectively, for the CP event and a negative anomaly for the EP event. During the development phase, there is no clear difference between both types of event, although the enhancement of the ER activity around July for the EP event is obvious.

We now discuss the limitation associated with the compositing procedure. Considering the limited number of events, the high significance (estimated using the bootstrap method) of the difference between the EP and CP composites is hardly reached (cf. Fig. 3). Of course, the significance of each composite considered separately is higher, especially for the EP composite (not shown). The 75% level used here for the significance of the difference between the composites allows us to highlight the most likely differences between the EP and CP El Niño composites. Such compositing procedure problem arises not only from the limited number of events, but also from the diversity of the evolution of events in the reanalyses over the period of interest and the difficulty in classifying them into two distinct groups. In fact, Kug et al. (2009), based on the NCEP Reanalysis, introduced three types of El Niño (i.e., CP, EP, and a mixed type). For instance, the last El Niño to date that took place in 2009/10 can be categorized as a CP El Niño (Kim et al. 2011) but its ocean dynamical behavior resembles the EP El Niño. Yu et al. (2011) propose defining the CP El Niño and mixed-type El Niño based on subsurface indexes that are more appropriate to capture the specificities of the events and to account for the large

diversity of El Niño types in nature. Takahashi et al. (2011) also propose classifying ENSO events in terms of their privileged dynamical regimes rather than from the historical SST indices like in Yeh et al. (2009). Their approach, like the one in Kao and Yu (2009), has the advantage of providing independent indices (i.e., uncorrelated) to separate the ENSO variability. We have verified here that the use of the indices of Takahashi et al. (2011) also leads to a different seasonal evolution of the relationship between ITV and ENSO for both types of events (cf. Fig. 4), which somehow supports the results of the composite analysis. We also verified that the results obtained from the composites hold for the two individual El Niños that are often considered as the archetypes of the EP and CP events, namely the 1997/98 El Niño and the 2004/05 El Niño, respectively (not shown). To gain confidence in the latter, longer datasets will still have to be used. These can be provided from coupled general circulation models (CGCMs) that can simulate realistically both the components of the ITV and the modulation of ENSO, considering that current generation models have difficulties in simulating these two aspects of the tropical variability [cf. Lin et al. (2006) for the ITV and Yu and Kim (2010a) for the El Niño types]. The mode selection in current models, whether CP or EP, is also very clearly separated compared to the observations (Kug et al. 2010; Dewitte et al. 2012). Our future plan is to investigate whether the new generation of CGCMs [Coupled Model Intercomparison Project Phase 5 (CMIP5)] can help overcome such a limitation. Our results also call for a better understanding of the forced oceanic response to the various patterns of the ITV during the two flavors of El Niño. This could be done following Shinoda et al. (2008), that is, based on forced ocean model experiments for which the ITV pattern under interest is considered in the atmospheric forcing of the model.

Acknowledgments. We are grateful to Dr. Matthew Wheeler for providing the code for space–time spectral analysis. We would like also to thank Pavel Konstantinov (Univ. of Moscow) for his computational assistance. We are grateful to Dr. Ben Giese from Texas A&M University for providing the 5-day-mean SODA data. Dr. D. Gushchina was supported by CNRS while visiting LEGOS in June 2011. The three anonymous reviewers are thanked for their constructive comments.

REFERENCES

Ashok, K., S. K. Behera, S. A. Rao, H. Weng, and T. Yamagata, 2007: El Niño Modoki and its possible teleconnection. *J. Geophys. Res.,* **112,** C11007, doi:10.1029/2006JC003798.

Bergman, J. W., H. H. Hendon, and K. M. Weickmann, 2001: Intraseasonal air–sea interactions at the onset of El Niño. *J. Climate,* **14,** 1702–1719.

Björnsson, H., and S. A. Venegas, 1997: A manual for EOF and SVD analyses of climatic data. CCGCR Rep. 97-1, McGill University, Montréal, QC, Canada, 52 pp.

Carton, J. A., and B. S. Giese, 2008: A reanalysis of ocean climate using Simple Ocean Data Assimilation (SODA). *Mon. Wea. Rev.,* **136,** 2999–3017.

Dewitte, B., G. Reverdin, and C. Maes, 1999: Vertical structure of an OGCM simulation of the equatorial Pacific Ocean in 1985–94. *J. Phys. Oceanogr.,* **29,** 1542–1570.

——, S. Purca, S. Illig, L. Renault, and B. Giese, 2008: Low-frequency modulation of the intraseasonal equatorial Kelvin wave activity in the Pacific Ocean from SODA: 1958–2001. *J. Climate,* **21,** 6060–6069.

——, J. Choi, S.-I. An, and S. Thual, 2012: Vertical structure variability and equatorial waves during central Pacific and eastern Pacific El Niños in a coupled general circulation model. *Climate Dyn.,* **38,** 2275–2289.

Efron, B., Ed., 1982: *The Jackknife, the Bootstrap, and Other Resampling Plans. CBMSNSF Monogr.,* No. 38, Society for Industrial and Applied Mathematics, 92 pp.

Eisenman, I., L. Yu, and E. Tziperman, 2005: Westerly wind bursts: ENSO's tail rather than the dog? *J. Climate,* **18,** 5224–5238.

Giese, B. S., and D. E. Harrison, 1991: Eastern equatorial Pacific response to three composite westerly wind types. *J. Geophys. Res.,* **96** (Suppl.), 3239–3248.

Gill, A. E., 1980: Some simple solutions for heat induced tropical circulation. *Quart. J. Roy. Meteor. Soc.,* **106,** 447–462.

Gushchina, D., and B. Dewitte, 2011: The relationship between intraseasonal tropical variability and ENSO and its modulation at seasonal to decadal timescales. *Cent. Eur. J. Geosci.,* **3** (2), 175–196.

Hartten, L. M., 1996: Synoptic settings of westerly wind bursts. *J. Geophys. Res.,* **101,** 16 997–17 019.

Hendon, H. H., B. Liebmann, and J. D. Glick, 1998: Oceanic Kelvin waves and the Madden–Julian oscillation. *J. Atmos. Sci.,* **55,** 88–101.

——, C. Zhang, and J. D. Glick, 1999: Interannual variation of the Madden–Julian oscillation during austral summer. *J. Climate,* **12,** 2538–2550.

——, M. C. Wheeler, and C. Zhang, 2007: Seasonal dependence of the MJO–ENSO relationship. *J. Climate,* **20,** 531–543.

Kalnay, E., and Coauthors, 1996: The NCEP/NCAR 40-Year Reanalysis Project. *Bull. Amer. Meteor. Soc.,* **77,** 437–471.

Kao, H.-Y., and J.-Y. Yu, 2009: Contrasting eastern-Pacific and central-Pacific types of ENSO. *J. Climate,* **22,** 615–632.

Kessler, W. S., M. J. McPhaden, and K. M. Weickmann, 1995: Forcing of intraseasonal Kelvin waves in the equatorial Pacific. *J. Geophys. Res.,* **100,** 10 613–10 631.

Kiladis, G. N., and M. Wheeler, 1995: Horizontal and vertical structure of observed tropospheric equatorial Rossby waves. *J. Geophys. Res.,* **100** (D11), 22 981–22 997.

Kim, W., S.-W. Yeh, J.-H. Kim, J.-S. Kug, and M. Kwon, 2011: The unique 2009–2010 El Niño event: A fast phase transition of warm pool El Niño to La Niña. *Geophys. Res. Lett.,* **38,** L15809, doi:10.1029/2011GL048521.

Kistler, R., and Coauthors, 2001: The NCEP–NCAR 50-Year Reanalysis: Monthly means CD-ROM and documentation. *Bull. Amer. Meteor. Soc.,* **82,** 247–267.

Kug, J.-S., F.-F. Jin, K. P. Sooraj, and I.-S. Kang, 2008: State development atmospheric noise associated with ENSO. *Geophys. Res. Lett.,* **35,** L05701, doi:10.1029/2007GL032017.

——, ——, and S.-I. An, 2009: Two types of El Niño events: Cold tongue El Niño and warm pool El Niño. *J. Climate,* **22,** 1499–1515.

——, J. Choi, S.-I. An, F.-F. Jin, and A.-T. Wittenberg, 2010: Warm pool and cold tongue El Niño events as simulated by the GFDL2.1 coupled GCM. *J. Climate,* **23,** 1226–1239.

Larkin, N. K., and D. E. Harrison, 2005: Global seasonal temperature and precipitation anomalies during El Niño autumn and winter. *Geophys. Res. Lett.,* **32,** L13705, doi:10.1029/2005GL022738.

Lau, W. K. M., 2005: El Niño Southern Oscillation connection. *Intraseasonal Variability of the Atmosphere-Ocean Climate System,* W. K. M. Lau and D. E. Waliser, Eds., Praxis Publishing, 71–300.

Liebmann, B., H. H. Hendon, and J. D. Glick, 1994: The relationship between tropical cyclones of the western Pacific and Indian Oceans and the Madden-Julian oscillation. *J. Meteor. Soc. Japan,* **72,** 401–411.

Lin, J.-L., and Coauthors, 2006: Tropical intraseasonal variability in 14 IPCC AR4 climate models. Part I: Convective signals. *J. Climate,* **19,** 2665–2690.

Lin, J. W.-B., J. D. Neelin, and N. Zeng, 2000: Maintenance of tropical intraseasonal variability: Impact of evaporation–wind feedback and midlatitude storms. *J. Atmos. Sci.,* **57,** 2793–2823.

Madden, R., and P. Julian, 1972: Description of global-scale circulation cells in the tropics with a 40–50 day period. *J. Atmos. Sci.,* **29,** 1109–1123.

Maloney, E. D., and D. L. Hartmann, 2001: The Madden–Julian oscillation, barotropic dynamics, and North Pacific tropical cyclone formation. Part I: Observations. *J. Atmos. Sci.,* **58,** 2545–2558.

Matthews, A. J., and G. N. Kiladis, 1999: Interactions between ENSO, transient circulation, and tropical convection over the Pacific. *J. Climate,* **12,** 3062–3086.

McPhaden, M. J., 1999: Genesis and evolution of the 1997–98 El Niño. *Science,* **283,** 950–954.

——, and Coauthors, 1998: The Tropical Ocean-Global Atmosphere observing system: A decade of progress. *J. Geophys. Res.,* **103,** 14 169–14 240.

Philander, S. G. H., 1978: Instabilities of zonal equatorial currents, 2. *J. Geophys. Res.,* **83** (C7), 3679–3682.

Rasmusson, E., and T. Carpenter, 1982: Variations in the tropical sea surface temperature and surface wind fields associated with the Southern Oscillation/El Niño. *Mon. Wea. Rev.,* **110,** 354–384.

Rayner, N. A., D. E. Parker, E. B. Horton, C. K. Folland, L. V. Alexander, D. P. Rowell, E. C. Kent, and A. Kaplan, 2003: Global analyses of sea surface temperature, sea ice, and night marine air temperature since the late nineteenth century. *J. Geophys. Res.,* **108,** 4407, doi:10.1029/2002JD002670.

Roundy, P. E., and G. N. Kiladis, 2006: Observed relationship between oceanic Kelvin waves and atmospheric forcing. *J. Climate,* **19,** 5253–5272.

——, and J. R. Kravitz, 2009: The association of the evolution of intraseasonal oscillations to ENSO phase. *J. Climate,* **22,** 381–395.

Seiki, A., and Y. N. Takayabu, 2007a: Westerly wind bursts and their relationship with intraseasonal variations and ENSO. Part I: Statistics. *Mon. Wea. Rev.,* **135,** 3325–3345.

——, and ——, 2007b: Westerly wind bursts and their relationship with intraseasonal variations and ENSO. Part II: Energetics over the western and central Pacific. *Mon. Wea. Rev.,* **135,** 3346–3361.

——, ——, K. Yoneyama, N. Sato, and M. Yoshizaki, 2009: The oceanic response to the Madden-Julian oscillation and ENSO. *Sci. Online Lett. Atmos.,* **5,** 93–96, doi:10.2151/sola.2009-024.

Shinoda, T., P. E. Roundy, and G. N. Kiladis, 2008: Variability of intraseasonal Kelvin waves in the equatorial Pacific Ocean. *J. Phys. Oceanogr.,* **38,** 921–944.

Slingo, J. M., D. P. Rowel, and K. R. Sperber, 1999: On the predictability of the interannual behavior of the Madden-Julian Oscillation and its relationship with El Niño. *Quart. J. Roy. Meteor. Soc.,* **125,** 583–609.

Sokolikhina, E. V., E. K. Semenov, and N. N. Sokolikhina, 2006: The atmospheric circulation on the synoptic scale during the culmination phase of the El-Niño–Southern Oscillation events (1997–1998). *Adv. Geosci.*, **6,** 17–21.

Spiegel, M. R., 1990: *Schaum's Outline of Theory and Problems of Statistics*. McGraw-Hill, 504 pp.

Takahashi, K., A. Montecinos, K. Goubanova, and B. Dewitte, 2011: ENSO regimes: Reinterpreting the canonical and Modoki El Niño. *Geophys. Res. Lett.,* **38,** L10704, doi:10.1029/2011GL047364.

Tang, Y., and B. Yu, 2008: MJO and its relationship to ENSO. *J. Geophys. Res.,* **113,** D14106, doi:10.1029/2007JD009230.

Waliser, D., 2005: Predictability and forecasting. *Intraseasonal Variability in the Atmosphere-Ocean Climate System,* W. K. M. Lau and D. E. Waliser, Eds., Springer, 389–418.

——, K. M. Lau, W. Stern, and C. Jones, 2003: Potential predictability of the Madden–Julian oscillation. *Bull. Amer. Meteor. Soc.,* **84,** 33–50.

Weickmann, K. M., 1991: El Niño Southern Oscillation and the Madden-Julian (30–60 day) oscillation during 1981–82. *J. Geophys. Res.,* **96,** 3187–3196.

Wheeler, M. C., and G. N. Kiladis, 1999: Convectively coupled equatorial waves: Analysis of clouds and temperature in the wavenumber–frequency domain. *J. Atmos. Sci.,* **56,** 374–399.

——, and K. M. Weickmann, 2001: Real-time monitoring and prediction of modes of coherent synoptic to intraseasonal tropical variability. *Mon. Wea. Rev.,* **129,** 2677–2694.

——, and J. L. McBride, 2005: Australian–Indonesian monsoon. *Intraseasonal Variability in the Atmosphere-Ocean Climate System,* W. K. M. Lau and D. E. Waliser, Eds., Springer, 125–168.

Yasunari, T., 1979: Cloudiness fluctuations associated with the northern hemisphere summer monsoon. *J. Meteor. Soc. Japan,* **57,** 227–242.

Yeh, S.-W., S.-J. Kug, B. Dewitte, M.-H. Kwon, B. P. Kirtman, and F.-F. Jin, 2009: El Niño in a changing climate. *Nature,* **461,** 511–514.

Yu, J.-Y., and H.-Y. Kao, 2007: Decadal changes of ENSO persistence barrier in SST and ocean heat content indices: 1958-2001. *J. Geophys. Res.,* **112,** D13106, doi:10.1029/2006JD007654.

——, and S. T. Kim, 2010a: Identification of Central-Pacific and Eastern-Pacific types of ENSO in CMIP3 models. *Geophys. Res. Lett.,* **37,** L15705, doi:10.1029/2010GL044082.

——, and ——, 2010b: Three evolution patterns of Central-Pacific El Niño. *Geophys. Res. Lett.,* **37,** L08706, doi:10.1029/2010GL042810.

——, and ——, 2011: Relationships between extratropical sea level pressure variations and the central Pacific and eastern Pacific types of ENSO. *J. Climate,* **24,** 708–720.

——, H.-Y. Kao, and T. Lee, 2010: Subtropics-related interannual sea surface temperature variability in the central equatorial Pacific. *J. Climate,* **23,** 2869–2884.

——, ——, ——, and S. Kim, 2011: Subsurface ocean temperature indices for central-Pacific and eastern-Pacific types of El Niño and La Niña events. *Theor. Appl. Climatol.,* **103,** 337–344.

Zhang, C., 2005: Madden-Julian Oscillation. *Rev. Geophys.,* **43,** RG2003, doi:10.1029/2004RG000158.

——, and J. Gottschalck, 2002: SST anomalies of ENSO and the Madden–Julian oscillation in the equatorial Pacific. *J. Climate,* **15,** 2429–2445.